Title: Inferring drivers of changing land surface phenology from Landsat time series

Authors: Cornelius Senf and Tobias Krueger

Affiliation: Integrative Research Institute on Transformation of Human-Environment Systems (IRI THESys), Humboldt-Universität zu Berlin, Unter den Linden 6, 10099 Berlin, Germany

Correspondence to: Cornelius Senf; Tel: +49 151 50652760; E-Mail: corneliussenf@googlemail.com

Keywords: Phenology; Remote sensing; Climate change; Bayesian hierarchical modelling; Landsat

Abstract: Phenology is an important ecosystem property, and monitoring and modeling of phenology is particularly important for understanding climate change impacts on vegetated ecosystems. However, in-situ measurements are frequently confined to a few specific observation sites and species, and are thus limited for fully understanding the drivers of changing phenology at broader scales. Moderate resolution remote sensing time series from the Landsat archive can help overcome this limitation by delivering a consistent estimate of land surface phenology over the past 30 years. Yet, methods for inferring the drivers of variation in land surface phenology from these data remain scarce. We here present a new model for inferring drivers of changing land surface phenology from Landsat time series. We demonstrate our model using a case study comprising broadleaved and coniferous forests and estimating the effects of pre-season temperature and winter-chilling on inter-annual variation in the start of season. We identified significant effects of pre-season temperature on inter-annual variation in start of season, with a -3.74 d $°C^{-1}$ earlier start of season for broadleaved and a -2.68 d $°C^{-1}$ earlier start of season for coniferous forests, respectively. This relationship, however, was modulated by the number of chilling days, with a decreasing effect of pre-season temperature with decreasing number of chilling days. The inter-annual variation in start of season predicted from our model – i.e., calibrated solely from Landsat satellite time series – showed good agreement with in-situ observations of bud-break (Pearson's r = 0.79/RMSE = 4.88 d for broadleaved forests and r = 0.62/RMSE = 6.57 d for coniferous forests). Our model thus allows for inferring drivers of changing land surface phenology directly from Landsat time series, opening up phenological research in areas where in-situ measurements are unavailable, and at spatial and temporal scales difficult to tackle with field and coarse-scale remote sensing data.

Introduction

Phenology is a key property of ecosystems (Forrest & Miller-Rushing, 2010). Due to its sensitivity to climate, phenology is also a valuable indicator of climate change (Cleland, Chuine, Menzel, Mooney, & Schwartz, 2007). Climate change effects on vegetation phenology have been documented in numerous experimental and observational studies, finding shifts in the start of the growing season in many plant species as a result of climate change (Cleland et al., 2007; Menzel et al., 2006; Parmesan & Yohe, 2003). Those changing phenological patterns have profound impacts on ecosystem functions, such as carbon uptake (Keenan et al., 2014). In order to better understand the impacts of changing phenology on ecosystem function, it is fundamental to monitor, model and ultimately predict vegetation phenological dynamics at varying spatial and temporal scales (Pau et al., 2011; Tang et al., 2016).

A key data source for monitoring and modeling phenological dynamics are in-situ phenological measurements. Those measurements are generally taken at the level of individuals (e.g., single trees or plants), and the resulting information is used to calibrate species-specific phenological models that predict phenological phases (e.g., leaf unfolding) based on a set of aggregated meteorological variables (Basler, 2016; Chuine, 2000; Hufkens, Basler, Milliman, Melaas, & Richardson, 2018). However, such species-specific models are often difficult to regionalise to the ecosystem scale (Y. Fu, Zhang, Dong, & Yuan, 2014; Richardson et al., 2012; Tang et al., 2016), particularly if the exact species or community composition are unknown (Jeremy I. Fisher, Richardson, & Mustard, 2007). Further, calibrating species-specific models across large geographic extents is challenging, as in-situ phenological observations are lacking in many regions worldwide, or are difficult to compare due to varying measurement protocols and/or target species (Fitchett, Grab, & Thompson, 2015). An improved understand of phenological dynamics at the ecosystem scale is, however, required for further developing the representation of phenology in global vegetation models

(Richardson et al., 2012; Yang, Mustard, Tang, & Xu, 2012). Remote sensing, which measures so-called land surface phenology and thus delivers an integrated view on phenology independent of individual species (Morisette et al., 2009), might help overcoming this knowledge gap.

Classical approaches tracking phenology from remote sensing data made use of the synoptic view of the Advanced Very High Resolution Radiometer (AVHRR) sensor family (M. A. White et al., 2009). AVHRR, however, has a spatial resolution that is too coarse (1 km) to infer phenological dynamics in spatially heterogeneous landscapes. The MODerate Imaging Spectroradiometer (MODIS), which has a higher spatial resolution of 250 m, might improve the estimation of spatial drivers (Friedl et al., 2014), yet its short time series (starting in 2001) makes it difficult to infer temporal trends in phenological dynamics. Dense Landsat time series were recently suggested to overcome the limitations of MODIS and AVHRR in monitoring vegetation phenology (J. I. Fisher & Mustard, 2007; J. I. Fisher, Mustard, & Vadeboncoeur, 2006; Melaas, Friedl, & Zhu, 2013; Melaas, Sulla-Menashe, & Friedl, 2018; Senf, Pflugmacher, Heurich, & Krueger, 2017), since they have a medium spatial resolution of 30 m and cover a time-span of more than 30 years (from 1984 onwards). However, methods for inferring patterns and drivers of land surface phenology from those medium resolution sensors remain scarce.

We here present a new model for inferring drivers of inter-annual variation in land surface phenology from Landsat time series. Our model, which is based on a Bayesian hierarchical setup (Senf et al., 2017), integrates Landsat time series and meteorological observations, thus allowing for the direct assessment of drivers (e.g., pre-season temperature) on inter-annual variability in phenological parameters (e.g., the start of season). We demonstrate our model using a case study from southern Germany comprising broadleaved and coniferous forests. Our specific objectives were to (1) estimate the effects of pre-season temperature and winter chilling on inter-annual variability in start of season in broadleaved

and coniferous forests and to (2) compare the model, which is calibrated solely from Landsat time series, to in-situ phenological observations of leaf unfolding.

Model description

Landsat phenological model

The underlying Landsat phenological model utilized in this study follows previous work described in Melaas et al. (2013) and Senf et al. (2017) and can be summarised as follows: Consider a time series of Landsat images for which a vegetation index has been calculated. For a pixel i, all available vegetation index values can be pooled into a vector $\boldsymbol{y}_{ti}$ sorted by observation day of year t (see Fig. 1). The vector $\boldsymbol{y}_{ti}$ thus describes the phenological variation of pixel i, independent of the year of observation, which may be modeled as $\boldsymbol{y}_{ti} \sim N(g(t;\, \boldsymbol{\beta}_i), \sigma^2)$. Thus, the mean phenological dynamics are described by a functional relationship $g(t;\, \boldsymbol{\beta}_i)$, with a set of parameters for each pixel $\boldsymbol{\beta}_i$. We here chose a logistic function as the base phenological model (Elmore, Guinn, Minsley, & Richardson, 2012; K. White, Pontius, & Schaberg, 2014):

$$g(t;\, \boldsymbol{\beta}_i) = \beta_{1[i]} + \frac{\beta_{2[i]}}{\left(1 + e^{-\beta_{3[i]} * (t - \beta_{4[i]})}\right)} \quad (1)$$

with $\boldsymbol{\beta}_i$ presenting a four-dimensional vector of model parameters describing the shape of the logistic function for each pixel i (see Figure 1 and Table 1). The parameter vector $\boldsymbol{\beta}_i$ is modelled as a multivariate normal distribution $MVN(\boldsymbol{\mu}_{[i]}, \boldsymbol{\Sigma}_\beta)$, with $\boldsymbol{\mu}_{[i]}$ being the vector of mean model parameters and $\boldsymbol{\Sigma}_\beta$ being the variance-covariance matrix of the four model parameters. Following Senf et al. (2017) we re-parameterized the multivariate normal distribution as $\boldsymbol{\beta}_i = (diag(\boldsymbol{\sigma}_\beta^2 * \boldsymbol{\tau}) * L_\beta * \boldsymbol{z}_\beta)^T + \boldsymbol{\mu}_{[i]}$ to numerically improve sampling (Monnahan, Thorson, & Branch, 2017). Thereby, $\boldsymbol{z}_\beta$ represents a vector of $N(0, 1)$ random variables, $\boldsymbol{\sigma}_\beta^2$ is a vector of variances, $\boldsymbol{\tau}$ represents a vector with scaling factors for the variance (which is by default set to $\boldsymbol{\tau} = \{0.1, 0.1, 0.1, 1\}$), and L_β is the Cholesky

decomposition of the correlation matrix C_β with $C_\beta = L_\beta * L_\beta{}^T$. The vector $\boldsymbol{\mu}_{[i]}$ centers the multivariate normal distribution on the approximate location of each phenological parameter in $\boldsymbol{\beta}_i$ and must be given *a priori*. We introduce an automatic algorithm for determining those prior choices in Section 2.3. A weakly-informative $half - cauchy(0, 1)$ prior is assigned to $\boldsymbol{\sigma}_\beta^2$ and a weakly-informative $LKJ(2)$ prior is assigned to the correlation matrix C_β.

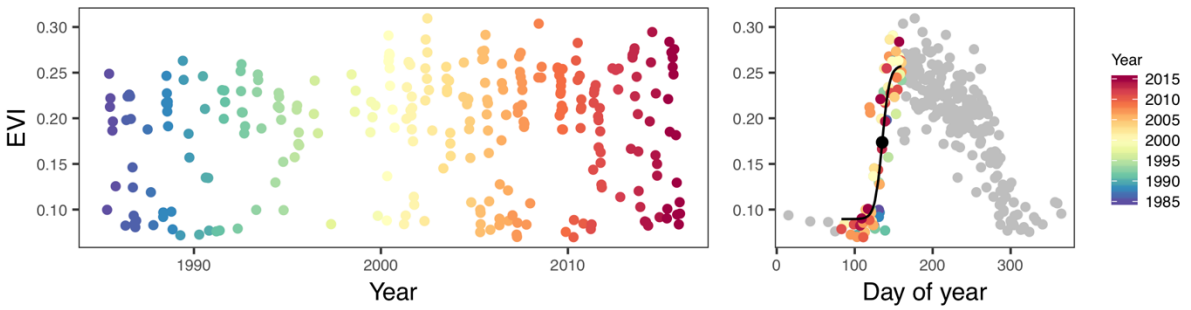

Figure 1: Example pixel time series showing the annual observations (left panel) and the pooled time series (right panel). Shown here is the Enhanced Vegetation Index (EVI). The pooled time series is truncated to spring and summer observations as described in Section 2.3, and only those observations are colored. A phenological model as described in Section 2.1 was fit to the data. The black dot represents the start of season estimated from the model.

Table 1: Phenological parameters of the model.

Parameter	Name	Description
$\beta_{1[i]}$	Minimum	The minimum spectral value.
$\beta_{2[i]}$	Magnitude	The magnitude of spectral change during the year.
$\beta_{3[i]}$	Change rate	The change rate in the inflection point.
$\beta_{4[i]}$	Start of season	The day of year of the inflection point.

Hierarchical formulation to model inter-annual variability

To account for temporal variation in the model parameters $\boldsymbol{\beta}_i$ among years j, we follow Senf et al. (2017) and replace $\boldsymbol{\beta}_i$ by a hierarchical level: $\boldsymbol{\beta'}_{ij} = \boldsymbol{\beta}_i + \boldsymbol{\phi}_j$. This hierarchical formulation allows the model parameters to simultaneously vary in space and time. We model $\boldsymbol{\phi}_j$ as a multivariate normal distribution $MVN(\boldsymbol{\gamma}_{[j]}, \boldsymbol{\Sigma}_{\phi})$, re-parameterized as described above: $\boldsymbol{\phi}_j = (diag(\boldsymbol{\sigma}_{\boldsymbol{\phi}}^2 * \boldsymbol{\tau}) * L_{\boldsymbol{\phi}} * \boldsymbol{z}_{\boldsymbol{\phi}})^T + \boldsymbol{\gamma}_{[j]}$. While previous studies assumed the temporal variation in model parameters to be purely random (Senf et al., 2017), that is setting $\boldsymbol{\gamma}_{[j]}$ to {0,0,0,0}, we here test the hypothesis that the temporal variation in the start of season $\gamma_{4[j]}$ is described by a linear combination of annual predictor variables $\gamma_{4[j]} = \boldsymbol{M}_j\boldsymbol{\rho}$; with $\boldsymbol{\rho}$ being a vector of model coefficients and $\boldsymbol{M}_i$ a design matrix of predictors. The sub-model thus determines the direction and strength of influence of a set of temporal drivers on the inter-annual variability in the start of season. The other model parameters (minimum, maximum or green-up rate; see Figure 1 and Table 1) could also be modeled dependent on temporal drivers. Weakly-informative $half-Cauchy(0,1)$ priors were assigned to the variance parameter $\boldsymbol{\sigma}_{\boldsymbol{\phi}}^2$, a weakly-informative $LKJ(2)$ prior was put on the correlation matrix $C_{\boldsymbol{\phi}}$, and weakly-informative $student-t(3,0,1)$ priors were assigned to $\boldsymbol{\rho}$.

Ensemble implementation and Bayesian inference

Bayesian hierarchical models are computational intensive and hence restricted to a limited number of pixels. However, previous research has shown that already a small number of pixels (e.g., 100 pixels) are sufficient for estimating the ecosystem-scale temporal dynamics in phenology (Senf et al., 2017). Hence, we here again utilize a sample of Landsat time series for estimating temporal dynamics and drivers of land surface phenology instead of creating wall-to-wall maps. However, to reduce bias stemming from sampling variability, we implemented an ensemble sampling strategy that draws m samples of size n, and later average over the m joint posterior probability distributions of each model parameter of

interest (i.e., $\boldsymbol{\phi}_j$ and $\boldsymbol{\rho}$). That way, we reduce bias in parameter estimates stemming from sampling variability, while simultaneously allowing for efficient and fast inference. The associated cost of greater imprecision of parameter estimates due to the averaging of the posterior distributions of the ensemble was mitigated by a sufficient number of ensemble members (Figure S1).

For each sampled time series, there was first need for selecting only spring and summer observations. We follow a method suggested by Melaas et al. (2013), which excludes all observations before day of year 80 (winter observations) and then uses an iterative algorithm identifying the transition from summer to autumn. In essence, the algorithm fits a linear model to a running window of 21 observations and identifies the day of year with the first negative slope as the summer-autumn transition date.

Prior choices for $\boldsymbol{\mu}_{[i]}$ are estimated by iteratively fitting $g(t;\ \boldsymbol{\beta}_i)$ using non-linear least squares until 10 models were collected (models that did not converge were dropped). We then averaged parameter estimates over those 10 models and used the averages for $\boldsymbol{\mu}_{[i]}$. The prior choices could also be based on previous studies or knowledge of the local phenological system, if available.

Finally, full Bayesian inference was made by sampling the joint posterior distribution using Markov Chain Monte Carlo (MCMC) methods implemented in the free software Stan (Carpenter et al., 2017). The joint posterior distribution was sampled independently for each of the m samples. Sampling was done using four chains à 4,000 iterations, of which 2,000 were later dropped as warm-up iterations. Convergence of chains was tested by comparing the between- and within-chain variance using the $\hat{R}$ statistic described in Gelman, Carlin, Stern, and Rubin (2014). Subsequently, we calculated average posterior distributions over all m joint posterior distributions. We tested the fit of the ensemble model by means of posterior predictive checking. Posterior predictive checking generates replicated data drawn randomly under the model, which can then be compared to the observed data (Gelman et al., 2014). If

the model fits the data well, there should be no systematic differences between the replicated data and the observed vegetation index time series.

Case study: Drivers of changing phenology in broadleaved and coniferous forests

Study landscape

The study system is located in the Bavarian Forest National park, with moderate topography ranging from approximately 300 to 1,800 meters in elevation (Figure 1). The ecosystem is characterized by mountain beech forests with *Fagus sylvatica* (European beech) being the leading species. Other broad-leaved tree species include *Acer pseudoplatanus* (Sycamore maple) or *Quercus robur* (English oak), but *F. sylvatica* is by far the most abundant. The higher elevation areas of the ecosystem, in turn, are covered by mountain spruce forests, consisting mainly of *Picea abies* (Norway spruce), with some *Abeis alba* (European silver fir) intermixed.

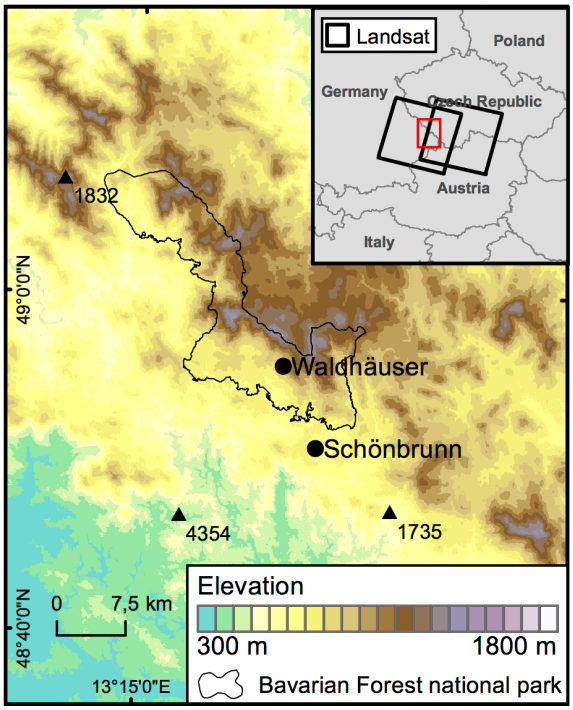

Figure 2: Study landscape with national park boundaries, the three meteorological stations (triangles), and the two in-situ phenological observation sites (points) from the International Phenological Gardens of Europe network.

194 ***Landsat data***

195 We identified suitable sampling locations for both broadleaved forests (i.e., mountain beech
196 forests) and coniferous forests (i.e., mountain spruce forests) using an existing land cover map
197 generated by National Park authorities from aerial imagery. To exclude young and/or
198 disturbed forests we only sampled mature stands, that is, stands with a minimum age of 60
199 years. The sample size was set to $n = 25$ and the number of samples in the ensemble was set
200 to $m = 10$. We also tested alternative sample and ensemble sizes, but found no substantial
201 differences in the results (data not shown). For each pixel sampled, cloud-, snow-, and
202 shadow-free EVI time series were generated from the full Landsat archive (see Senf et al.
203 (2017) for details on the Landsat processing). We preferred EVI over other vegetation indices
204 as it has been shown to allow better estimation of key phenological dates from remote sensing
205 data (Klosterman et al., 2014).

206 ***Temporal drivers of inter-annual variability in start of season***

207 Past research indicates substantial shifts in leave unfolding of the two major broadleaved and
208 coniferous tree species found in our study site under climate change (Menzel et al., 2006).
209 However, the underlying drivers are not fully understood. While warmer pre-season
210 temperatures likely support earlier leaf unfolding, warmer winters might have an inverse
211 effect on spring phenology due to the absence of winter chilling (Y. H. Fu, Zhao, et al., 2015).
212 We hence chose two climatological variables hypothesized to influence broadleaved and
213 coniferous land surface phenology in our study ecosystem: pre-season temperature, winter
214 chilling, and their interaction accounting for potential modulating effects of winter chilling on
215 pre-season temperature effects (Y. H. Fu, Piao, et al., 2015). Pre-season temperature was
216 defined as the average mean daily temperature T_{mean} in the months April and May, being the
217 approximate month of vegetation green-up in our study region (Senf et al., 2017). Winter
218 chilling was defined as the number of days with $0 < T_{mean} \leq 5\ ^\circ C$ as suggested by previous
219 studies (Y. H. Fu, Zhao, et al., 2015). Both climatic variables were generated from three

meteorological stations operated by the German Weather Service (station-ids: 1735, 1832, 4354; Figure 1; ftp://ftp-cdc.dwd.de/pub/CDC/observations_germany/climate/daily/kl/historical/). We calculated average time-series of both meteorological variables for the complete study site and there is hence no spatial variation in the meteorological variables among sampling locations. Finally, we restricted the time-series to our study period (1985 – 2015) and z-transformed the data to represent anomalies in units of standard deviation.

Comparison to in-situ measurements

After sampling the joint posterior distribution for each model in the ensemble and subsequently averaging over the ensemble, we evaluated the predictive power of the model by comparing the predicted inter-annual variability in the start of season against in-situ observations of leave unfolding recorded for each three *F. sylvatica* trees and three *P. abies* trees at two phenological gardens within and in close proximity to the National Park, respectively (see Figure 1). The phenological observations were acquired from the International Phenological Gardens of Europe network (stations: Waldhäuser and Schönbrunn; Figure 1; http://ipg.hu-berlin.de/).

Results

All models in the ensemble showed good convergence with $\hat{R}$ smaller 1.01 for 99% of the model parameters. Further, uncertainty in the posterior could be substantially reduced by our ensemble approach (Figure S1), with little additional changes in the posterior after seven iterations. Posterior predictive checks indicated no systematic deviation between simulated and raw values (Figure S2), and 96% of the raw values were within the 95% credible interval of the posterior simulations.

We identified substantial inter-annual variability in three out of four phenological parameters (Figure 3). The start of season and minimum EVI both showed similar trends across broadleaved and coniferous forests, with an earlier start of season and a higher

minimum EVI over time. There were also some very late years (e.g., 1991) and some very early years (e.g., 2007 and 2009) identifiable for both broadleaved and coniferous forests. No substantial inter-annual variability could be detected for the maximum EVI, yet there was a slight decreasing trend over time for coniferous forests and a slight increasing trend over time for broadleaved forests. Substantial inter-annual variability could also be detected for the green-up rate of broadleaved forests, whereas coniferous forests had more stable green-up rates over time.

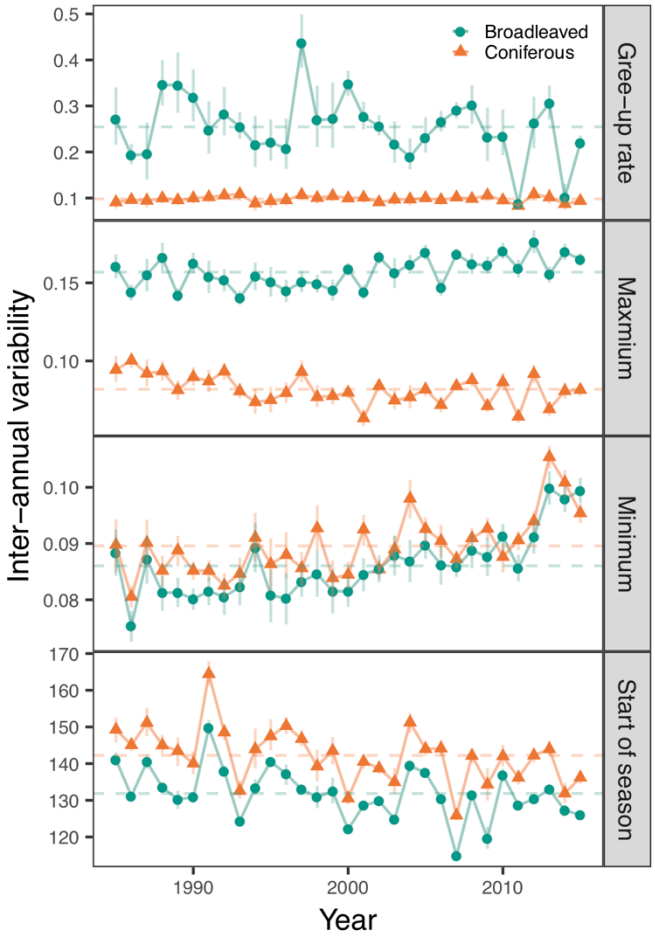

Figure 3: Ecosystem-scale inter-annual variability in the four phenological parameters estimated from Landsat time series for two forest types. Dots represent the median of the posterior distribution and error-bars extent from the 2.5% to the 97.5% quantile of the posterior (95% credible interval). The dashed horizontal lines indicate the long-term average.

The driver analysis revealed that the inter-annual variability in the start of season is highly sensitive to pre-season temperature (Figure 4), with a -3.74 d °C^{-1} earlier start of season for broadleaved and a -2.68 d °C^{-1} earlier start of season for coniferous forests, respectively. The effect of pre-season temperature on inter-annual variability in start of season was, however, modulated by the total number of chilling days in the preceding winter, with a decreasing effect of pre-season temperature on inter-annual variability in the start of season with a decreasing number of chilling days.

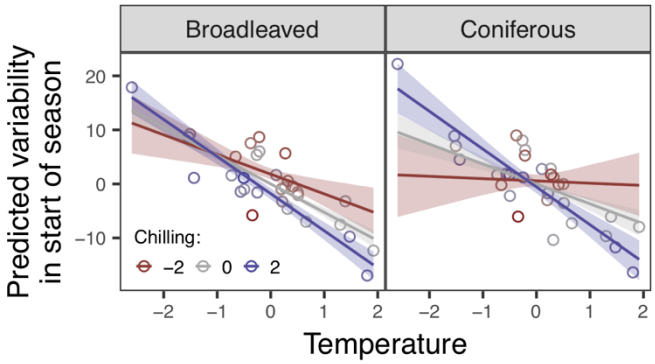

Figure 4: Ecosystem-scale inter-annual variability in start of season predicted from our model using pre-season temperature and winter chilling days as predictors. Both predictors are z-transformed and thus represent anomalies in standard deviations from the long-term average. Ribbons indicate the 95% credible interval.

Comparing predictions from the model (i.e., based on the regression relationship shown in Figure 4) to in-situ observations of bud-break (Figure 5), we found strong agreement for broadleaved forests (Pearson's r = 0.79 [0.74 – 0.80] and RMSE = 4.88 [4.60 – 5.21] days) and moderate agreement for coniferous forests (Pearson's r = 0.69 [0.63 – 0.75] and RMSE = 6.57 [6.00 – 7.13] days). Hence, our model – based only on pre-season temperature and winter chilling and calibrated solely from Landsat time series – was able to

predict the general inter-annual variability in spring phenology as recorded in in-situ measurements.

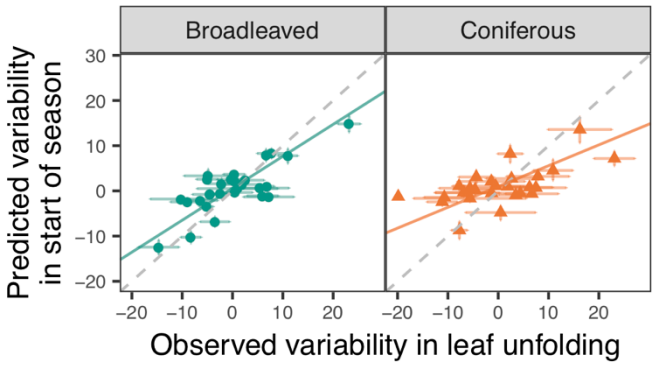

Figure 5: Comparing the ecosystem-scale inter-annual variability in start of season predicted from our model to in-situ observations of leaf unfolding derived from two phenological gardens in and around the national park (see Figure 2). Dots represent the median of the posterior (prediction; *y*-axis) and the arithmetic mean (leaf unfolding; *x*-axis). Uncertainty in the prediction is expressed by the 95% credible interval, whereas error-bars for the leaf unfolding represent 95% confidence intervals.

Discussion

We here presented a new model for inferring drivers of changing land surface phenology from Landsat time series. Our study is among the first to explicitly integrate Landsat time series with meteorological observations in order to deliver insights into the drivers underlying changing phenological patterns. Hence, instead of creating phenological products from remote sensing data that are subsequently used in analysis, we here suggest to calibrate phenological models directly from the millions of spectral observations available through long-term satellite archives such as Landsat. The advantage is a reduced number of, and redundancy in, processing steps, as well as a better propagation of uncertainty, which is otherwise largely neglected in remotely sensed phenological products. Moreover, given that the Landsat data used in this study have global coverage and are free to access, and considering emerging

cloud-computing capabilities like the Google Earth Engine (Gorelick et al., 2017), it is at the researchers fingertips to use Landsat for understanding phenological dynamics globally.

Integrating Landsat time series with meteorological observations allowed us to infer drivers of inter-annual variability in the start of season, building a predictive model that is solely calibrated from Landsat time series. While we here only modeled the start of season, any of the other parameters (i.e., minimum spectral index value, maximum spectral index value or green-up rate) could be modeled, too. As shown in our case study, the model was capable of predicting inter-annual variability in leaf-unfolding observed in-situ, despite the relatively simple model structure. This finding reinforces previous studies showing that more complex models do not necessarily lead to better predictions (Basler, 2016; Yang et al., 2012). In fact, RMSE values obtained by our model are in a similar range or even lower than comparable or more complex phenological models (Basler, 2016; Hufkens et al., 2018), emphasizing the predictive power of our model. Further, as our model is calibrated on land surface phenology (Morisette et al., 2009), it might better represent the ecosystem-scale drivers of phenology than models based on in-situ observations. This is mainly due to a more aggregated view going beyond individual species (Jeremy I. Fisher et al., 2007). This difference might be particularly important for calibrating phenological models used in global vegetation models (Richardson et al., 2012; Yang et al., 2012). Finally, in-situ phenological measurements themselves are often highly uncertain, with large differences among observations taken in close proximity (i.e., large confidence-intervals along the *x*-axis in Figure 5). This uncertainty, however, is often neglected in phenological models.

The drivers of inter-annual variability in start of season identified in this study largely corroborate the current literature, with pre-season temperature being a major control of spring phenology (Basler, 2016; Menzel et al., 2006; Yang et al., 2012). However, recent studies also showed a modulating effect of winter chilling on pre-season temperature effects (Y. H. Fu, Piao, et al., 2015), for which we found support in our study (Figure 4). Thus, even though

spring temperatures might further increase in the future, warming-related reductions in chilling days might slow down the advance of spring phenology under climate change (Y. H. Fu, Zhao, et al., 2015). Yet, the exact processes are still elusive and additional drivers such as precipitation or the previous year's phenology are discussed in the current literature (Y. H. Fu, Piao, et al., 2015; Y. S. Fu et al., 2014). Our model – in conjunction with global long-term satellite records from the Landsat archive – can be extended to include those drivers and thus offers great potential for understanding phenological responses under climate change in more detail, and for areas/time scales yet hardly covered alternative data sources.

Acknowledgements

Cornelius Senf and Tobias Krueger are both funded through IRI THESys by the German Excellence Initiative. We thank Prof. Dr. Frank-M. Chmielewski of Humboldt-Universität zu Berlin for access to the phenological observations.

Data and code accessibility

All data and code used in this publication are available for review at https://github.com/corneliussenf/phenoBayes_drivers and will be archived using https://zenodo.org/ after the paper has been accepted for publication.

References

Basler, D. (2016). Evaluating phenological models for the prediction of leaf-out dates in six temperate tree species across central Europe. *Agricultural and Forest Meteorology, 217*, 10-21. doi:10.1016/j.agrformet.2015.11.007

Carpenter, B., Gelman, A., Hoffman, M. D., Lee, D., Goodrich, B., Betancourt, M., . . . Riddell, A. (2017). Stan: A Probabilistic Programming Language. *Journal of Statistical Software, 76*(1), 1-32. doi:10.18637/jss.v076.i01

Chuine, I. (2000). A unified model for budburst of trees. *J Theor Biol, 207*(3), 337-347. doi:10.1006/jtbi.2000.2178

Cleland, E. E., Chuine, I., Menzel, A., Mooney, H. A., & Schwartz, M. D. (2007). Shifting plant phenology in response to global change. *Trends Ecol Evol, 22*(7), 357-365. doi:10.1016/j.tree.2007.04.003

Elmore, A. J., Guinn, S. M., Minsley, B. J., & Richardson, A. D. (2012). Landscape controls on the timing of spring, autumn, and growing season length in mid-Atlantic forests. *Global Change Biology, 18*(2), 656-674. doi:10.1111/j.1365-2486.2011.02521.x

Fisher, J. I., & Mustard, J. F. (2007). Cross-scalar satellite phenology from ground, Landsat, and MODIS data. *Remote Sensing of Environment, 109*(3), 261-273. doi:10.1016/j.rse.2007.01.004

Fisher, J. I., Mustard, J. F., & Vadeboncoeur, M. A. (2006). Green leaf phenology at Landsat resolution: Scaling from the field to the satellite. *Remote Sensing of Environment, 100*(2), 265-279. doi:10.1016/j.rse.2005.10.022

Fisher, J. I., Richardson, A. D., & Mustard, J. F. (2007). Phenology model from surface meteorology does not capture satellite-based greenup estimations. *Global Change Biology, 13*(3), 707-721. doi:10.1111/j.1365-2486.2006.01311.x

Fitchett, J. M., Grab, S. W., & Thompson, D. I. (2015). Plant phenology and climate change: Progress in methodological approaches and application. *Progress in Physical Geography, 39*(4), 460-482. doi:10.1177/0309133315578940

Forrest, J., & Miller-Rushing, A. J. (2010). Toward a synthetic understanding of the role of phenology in ecology and evolution. *Philos Trans R Soc Lond B Biol Sci, 365*(1555), 3101-3112. doi:10.1098/rstb.2010.0145

Friedl, M. A., Gray, J. M., Melaas, E. K., Richardson, A. D., Hufkens, K., Keenan, T. F., . . . O'Keefe, J. (2014). A tale of two springs: using recent climate anomalies to characterize the sensitivity of temperate forest phenology to climate change. *Environmental Research Letters, 9*(5). doi:Artn 054006
10.1088/1748-9326/9/5/054006

Fu, Y., Zhang, H., Dong, W., & Yuan, W. (2014). Comparison of phenology models for predicting the onset of growing season over the Northern Hemisphere. *PLoS One, 9*(10), e109544. doi:10.1371/journal.pone.0109544

Fu, Y. H., Piao, S., Vitasse, Y., Zhao, H., De Boeck, H. J., Liu, Q., . . . Janssens, I. A. (2015). Increased heat requirement for leaf flushing in temperate woody species over 1980-2012: effects of chilling, precipitation and insolation. *Glob Chang Biol, 21*(7), 2687-2697. doi:10.1111/gcb.12863

388 Fu, Y. H., Zhao, H., Piao, S., Peaucelle, M., Peng, S., Zhou, G., . . . Janssens, I. A. (2015).
389 Declining global warming effects on the phenology of spring leaf unfolding. *Nature,*
390 *526*(7571), 104-107. doi:10.1038/nature15402

391 Fu, Y. S., Campioli, M., Vitasse, Y., De Boeck, H. J., Van den Berge, J., AbdElgawad, H., . .
392 . Janssens, I. A. (2014). Variation in leaf flushing date influences autumnal senescence
393 and next year's flushing date in two temperate tree species. *Proc Natl Acad Sci U S A,*
394 *111*(20), 7355-7360. doi:10.1073/pnas.1321727111

395 Gelman, A., Carlin, J. B., Stern, H. S., & Rubin, D. B. (2014). *Bayesian data analysis* (Vol.
396 2): Chapman & Hall/CRC Boca Raton, FL, USA.

397 Gorelick, N., Hancher, M., Dixon, M., Ilyushchenko, S., Thau, D., & Moore, R. (2017).
398 Google Earth Engine: Planetary-scale geospatial analysis for everyone. *Remote*
399 *Sensing of Environment, 202*, 18-27. doi:10.1016/j.rse.2017.06.031

400 Hufkens, K., Basler, D., Milliman, T., Melaas, E. K., & Richardson, A. D. (2018). An
401 integrated phenology modelling framework in R. *Methods in Ecology and Evolution,*
402 *9*(5), 1276-1285. doi:10.1111/2041-210x.12970

403 Keenan, T. F., Gray, J., Friedl, M. A., Toomey, M., Bohrer, G., Hollinger, D. Y., . . .
404 Richardson, A. D. (2014). Net carbon uptake has increased through warming-induced
405 changes in temperate forest phenology. *Nature Climate Change, 4*(7), 598-604.
406 doi:10.1038/Nclimate2253

407 Klosterman, S. T., Hufkens, K., Gray, J. M., Melaas, E., Sonnentag, O., Lavine, I., . . .
408 Richardson, A. D. (2014). Evaluating remote sensing of deciduous forest phenology at
409 multiple spatial scales using PhenoCam imagery. *Biogeosciences, 11*(16), 4305-4320.
410 doi:10.5194/bg-11-4305-2014

411 Melaas, E. K., Friedl, M. A., & Zhu, Z. (2013). Detecting interannual variation in deciduous
412 broadleaf forest phenology using Landsat TM/ETM plus data. *Remote Sensing of*
413 *Environment, 132*, 176-185. doi:10.1016/j.rse.2013.01.011

414 Melaas, E. K., Sulla-Menashe, D., & Friedl, M. A. (2018). Multidecadal Changes and
415 Interannual Variation in Springtime Phenology of North American Temperate and
416 Boreal Deciduous Forests. *Geophysical Research Letters, 45*(6), 2679-2687.
417 doi:10.1002/2017gl076933

418 Menzel, A., Sparks, T. H., Estrella, N., Koch, E., Aasa, A., Ahas, R., . . . Zust, A. (2006).
419 European phenological response to climate change matches the warming pattern.
420 *Global Change Biology, 12*(10), 1969-1976. doi:10.1111/j.1365-2486.2006.01193.x

Monnahan, C. C., Thorson, J. T., & Branch, T. A. (2017). Faster estimation of Bayesian models in ecology using Hamiltonian Monte Carlo. *Methods in Ecology and Evolution, 8*(3), 339-348. doi:10.1111/2041-210x.12681

Morisette, J. T., Richardson, A. D., Knapp, A. K., Fisher, J. I., Graham, E. A., Abatzoglou, J., . . . Liang, L. (2009). Tracking the rhythm of the seasons in the face of global change: phenological research in the 21st century. *Frontiers in Ecology and the Environment, 7*(5), 253-260. doi:10.1890/070217

Parmesan, C., & Yohe, G. (2003). A globally coherent fingerprint of climate change impacts across natural systems. *Nature, 421*(6918), 37-42. doi:10.1038/nature01286

Pau, S., Wolkovich, E. M., Cook, B. I., Davies, T. J., Kraft, N. J. B., Bolmgren, K., . . . Cleland, E. E. (2011). Predicting phenology by integrating ecology, evolution and climate science. *Global Change Biology, 17*(12), 3633-3643. doi:10.1111/j.1365-2486.2011.02515.x

Richardson, A. D., Anderson, R. S., Arain, M. A., Barr, A. G., Bohrer, G., Chen, G. S., . . . Xue, Y. K. (2012). Terrestrial biosphere models need better representation of vegetation phenology: results from the North American Carbon Program Site Synthesis. *Global Change Biology, 18*(2), 566-584. doi:10.1111/j.1365-2486.2011.02562.x

Senf, C., Pflugmacher, D., Heurich, M., & Krueger, T. (2017). A Bayesian hierarchical model for estimating spatial and temporal variation in vegetation phenology from Landsat time series. *Remote Sensing of Environment, 194*, 155-160. doi:10.1016/j.rse.2017.03.020

Tang, J. W., Korner, C., Muraoka, H., Piao, S. L., Shen, M. G., Thackeray, S. J., & Yang, X. (2016). Emerging opportunities and challenges in phenology: a review. *Ecosphere, 7*(8), e01436-n/a. doi:ARTN e01436
10.1002/ecs2.1436

White, K., Pontius, J., & Schaberg, P. (2014). Remote sensing of spring phenology in northeastern forests: A comparison of methods, field metrics and sources of uncertainty. *Remote Sensing of Environment, 148*, 97-107. doi:10.1016/j.rse.2014.03.017

White, M. A., de Beurs, K. M., Didan, K., Inouye, D. W., Richardson, A. D., Jensen, O. P., . . . Lauenroth, W. K. (2009). Intercomparison, interpretation, and assessment of spring phenology in North America estimated from remote sensing for 1982-2006. *Global Change Biology, 15*(10), 2335-2359. doi:10.1111/j.1365-2486.2009.01910.x

455 Yang, X., Mustard, J. F., Tang, J. W., & Xu, H. (2012). Regional-scale phenology modeling
456 based on meteorological records and remote sensing observations. *Journal of*
457 *Geophysical Research-Biogeosciences, 117*(G3), n/a-n/a. doi:Artn G03029
458 10.1029/2012jg001977
459